Propagation and second-harmonic generation of electromagnetic waves in a coupled-resonator optical waveguide

Youg Xu, Reginald K. Lee, and Amnon Yariv

Department of Applied Physics, California Institute of Technology, MS 128-95, Pasadena, California 91125

Received June 11 1999; revised manuscript received October 18 1999

Using both the tight-binding approximation and the finite-difference time domain method, we analyze two types of coupled-resonator optical waveguide (CROW), a coupled-microdisks waveguide and a waveguide composed of coupled defect cavities in a two-dimensional photonic crystal. We find that the dispersion relation of the CROW band can be simply described by a small coupling parameter κ, and the spatial characteristics of the CROW modes remain the same as those of the single-resonator high Q modes. As applications of these unique properties, we demonstrate that CROW's can be utilized in constructing waveguides without cross talk and enhance the efficiency of second-harmonic generation. © 2000 Optical Society of America
[S0740-3224(00)01303-5]

OCIS codes: 190.2620, 190.4360, 230.7370, 130.2790.

I. INTRODUCTION

Two mechanisms have been proposed and used for optical waveguiding.[1] The most widely used is waveguiding by total internal reflection. Another mechanism, Bragg waveguiding, in which waveguiding is achieved through Bragg reflection from a periodic structure, has also been demonstrated.[1,2] Recently a new type of waveguide based on the coupling of optical resonators, the coupled-resonator optical waveguide (CROW), was proposed.[3] Figure 1 shows two CROW's that are based on different types of high-Q resonator. In Fig. 1(a) the individual high-Q resonator of the CROW is the defect cavity[4–6] embedded in a two-dimensional (2D) triangular lattice photonic crystal.[7–9] The building block of the CROW shown in Fig. 1(b), however, is the microdisk resonator.[10,11]

In both realizations of the CROW, we assume a sufficiently large separation between the high-Q resonators. Consequently the photons are tightly confined within each individual resonator and can propagate only by hopping from one resonator to its nearest neighbor. This is exactly the optical analog of the tight-binding limit in condensed-matter physics.[12] With this approximation, two important properties of the CROW have been shown[3] under the condition that the single-resonator high-Q mode is nondegenerate. First, the waveguide modes of CROW remain essentially the same as those of the high-Q modes in a single resonator and have the same symmetry characteristics. This unique property can be utilized to construct reflectionless bends,[3] and, as we shall see in Section 3 below, the CROW intersections without cross talk. Second, the dispersion relation of CROW's is greatly different from that of conventional dielectric waveguides and can be simply characterized by a coupling coefficient κ. In a weakly coupled CROW the optical waves are dramatically slowed down, a property that can be used to enhance the efficiency of nonlinear optical processes.[3] In this paper we generalize the analysis of Ref. 3 to allow for the degeneracy of the single-resonator high-Q modes. Then, using the finite-difference time domain[13,14] (FDTD) method, we numerically calculate the band structures and the waveguide modes of the two CROW's in Fig. 1 and compare the numerical results with the theoretical results of the tight-binding analysis.

The second-harmonic generation (SHG) process in photonic crystals or in defect cavities has been extensively discussed in the literature.[15–22] In photonic crystals, it has been shown that the second-harmonic field can be enhanced at the band edge of the photonic crystals, where the group velocity tends to zero.[15–18] In the case of defect cavities, the enhancement of SHG efficiency is achieved as a result of the large optical field amplitude of the localized defect-cavity modes.[20–22] However, both of the two properties, low group velocity and large optical field amplitude, can be simultaneously achieved in the CROW. Therefore, in this paper, as an example of the potential usefulness of CROW devices, we develop a general formalism for the SHG process in the CROW and apply this formalism to two specific SHG configurations. We calculate the SHG efficiency and show that it can be greatly enhanced in a CROW.

Besides in second-harmonic generation, the CROW might also be useful for many other applications in which reduced group velocity plays a critical role. For example, a CROW may be utilized to enhance stimulated emission, because the effective gain is proportional to $1/v_g$.[23,24] It also might find application as an optical delay line.[25] These possibilities, however, are not pursued in this paper.

This paper is organized as follows: In Section 2 we present the general formalism of the tight-binding approximation as applied to the CROW. In Section 3 the numerical results for the dispersion relations and mode characteristics of the coupled defect-cavity waveguide and the coupled microdisk waveguide are shown and dis-

0740-3224/2000/030387-14$15.00

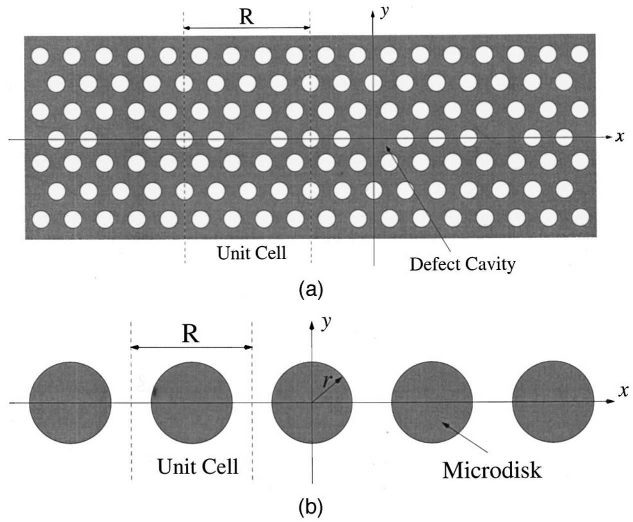

Fig. 1. Two examples of CROW. (a) A CROW composed of coupled defect cavities embedded in a 2D triangular lattice photonic crystal. R is the size of a unit cell, and $\mathbf{e}_x$ is the direction of the periodicity for the coupled resonators. (b) A CROW realized by coupling of the microdisks along the $\mathbf{e}_x$ direction. R is defined in the same way as for (a).

cussed. In Section 4 we present our theoretical analysis of the SHG process in the CROW. Finally, we summarize in Section 5.

2. TIGHT BINDING ANALYSIS OF CROW

In a single high-Q optical resonator, the eigenmode $\mathcal{E}_l(\mathbf{r})$ satisfies (in Gaussian units)

$$\nabla \times [\nabla \times \mathcal{E}_l(\mathbf{r})] = \epsilon_0(\mathbf{r}) \frac{\Omega_l^2}{c^2} \mathcal{E}_l(\mathbf{r}), \tag{1}$$

where Ω_l is the eigenfrequency of the lth mode and $\epsilon_0(\mathbf{r})$ represents the dielectric constant of the single resonator. The eigenmodes $\mathcal{E}_l(\mathbf{r})$ are also orthonormal:

$$\int \mathrm{d}\mathbf{r}\epsilon_0(\mathbf{r})\mathcal{E}_l(\mathbf{r}) \cdot \mathcal{E}_m(\mathbf{r}) = \delta_{l,m}, \tag{2}$$

where, as in Ref. 3, we take the Q factors of the resonator modes to be high and assume the mode function $\mathcal{E}_l(\mathbf{r})$ to be real.

In the spirit of the tight-binding approximation, we take the waveguide mode $\mathbf{E}_K(\mathbf{r}, t)$ of the CROW as a linear combination of the high-Q modes $\mathcal{E}_l(\mathbf{r})$ within the individual resonators along the $\mathbf{e}_x$ axis (see Fig. 1). Denoting the coordinate of the center of the nth resonator as $x = nR$, we have

$$\mathbf{E}_K(\mathbf{r}, t) = A \exp(i\omega_K t) \sum_{n,l} \exp(-inKR)\, b_l \mathcal{E}_l(\mathbf{r} - nR\mathbf{e}_x). \tag{3}$$

K in Eq. (3) is similar to the crystal momentum (divided by $\hbar$) of the electrons in solids. In this paper we shall call it the crystal momentum of the waveguide mode. It is straightforward to show that waveguide mode $\mathbf{E}_K(\mathbf{r}, t)$ satisfies the Bloch theorem. Consequently we can limit wave vector K to the first Brillouin zone, i.e., $-\pi/R \leqslant K \leqslant \pi/R$.

$\mathbf{E}_K(\mathbf{r}, t)$ also satisfies Maxwell's equations, which leads to

$$\nabla \times [\nabla \times \mathbf{E}_K] = \epsilon(\mathbf{r}) \frac{\omega_K^2}{c^2} \mathbf{E}_K, \tag{4}$$

where $\epsilon(\mathbf{r})$ is the dielectric constant of the coupled resonators and ω_K is the eigenfrequency of the waveguide mode.

After substituting Eq. (3) into Eq. (4), multiplying both sides from the left by $\mathcal{E}_m(\mathbf{r})$, and spatially integrating, we find the following eigenequation for mode expansion coefficient b_l:

$$\sum_l b_l \Omega_l^2 \left[\delta_{m,l} + \sum_{n \neq 0} \exp(-inKR) \beta_{m,l}^n \right] = \omega_K^2 \sum_l b_l \left[\delta_{m,l} + \Delta\alpha_{m,l} + \sum_{n \neq 0} \exp(-inKR) \alpha_{m,l}^n \right], \tag{5}$$

where $\alpha_{m,l}^n$, $\beta_{m,l}^n$, and $\Delta\alpha_{m,l}$ are defined as

$$\alpha_{m,l}^n = \int \mathrm{d}\mathbf{r}\epsilon(\mathbf{r})\mathcal{E}_m(\mathbf{r}) \cdot \mathcal{E}_l(\mathbf{r} - nR\mathbf{e}_x), \qquad n \neq 0, \tag{6a}$$

$$\beta_{m,l}^n = \int \mathrm{d}\mathbf{r}\epsilon_0(\mathbf{r} - nR\mathbf{e}_x)\mathcal{E}_m(\mathbf{r}) \cdot \mathcal{E}_l(\mathbf{r} - nR\mathbf{e}_x), \qquad n \neq 0, \tag{6b}$$

$$\Delta\alpha_{m,l} = \int \mathrm{d}\mathbf{r}[\epsilon(\mathbf{r}) - \epsilon_0(\mathbf{r})]\mathcal{E}_m(\mathbf{r}) \cdot \mathcal{E}_l(\mathbf{r}). \tag{6c}$$

If the coupling between the resonators is sufficiently weak, we can keep only the nearest-neighbor coupling, which means that $\alpha_{m,l}^n = \beta_{m,l}^n = 0$ if $n \neq \pm 1$. From symmetry considerations, we also require that $\alpha_{m,l}^1 = \alpha_{m,l}^{-1}$ and $\beta_{m,l}^1 = \beta_{m,l}^{-1}$. Putting these observations together yields, for Eq. (5),

$$\sum_l b_l \Omega_l^2 [\delta_{m,l} + 2\beta_{m,l}^1 \cos(KR)] = \omega_K^2 \sum_l b_l [\delta_{m,l} + \Delta\alpha_{m,l} + 2\alpha_{m,l}^1 \cos(KR)]. \tag{7}$$

Generally, if the single resonator has N degenerate or nearly degenerate high-Q modes $\mathcal{E}_l(\mathbf{r})$ with $l = 1, \dots, N$, we need to diagonalize the $N \times N$ matrix of Eq. (7) to find the dispersion relations of the CROW. The result generally depends on all the parameters $\alpha_{m,l}^1$, $\beta_{m,l}^1$, and $\Delta\alpha_{m,l}$ with $m, l = 1, \dots, N$.

However, if a single resonator possesses certain symmetries, the solution is usually much simpler. For example, each of the individual microdisks and defect cavities shown in Fig. 1 possesses a mirror reflection symmetry with respect to the $y = 0$ plane. Therefore the single resonator modes can be classified according to the parity P of this mirror reflection symmetry:

$$E_x(x, y, z) = PE_x(x, -y, z), \tag{8a}$$

$$E_y(x, y, z) = -PE_y(x, -y, z), \tag{8b}$$

$$E_z(x, y, z) = PE_z(x, -y, z), \tag{8c}$$

$$B_x(x, y, z) = -PB_x(x, -y, z), \tag{8d}$$

$$B_y(x, y, z) = PB_y(x, -y, z), \tag{8e}$$

$$B_z(x, y, z) = -PB_z(x, -y, z), \tag{8f}$$

where the parity P of the eigenmode can take the value of ± 1. The modes with $P = 1$ and $P = -1$ will be called, respectively, the even modes and the odd modes.

It has been shown that the high-Q modes in both the microdisk cavity and the single-defect cavity are doubly degenerate and have opposite parity.[6,10,11] Consequently, for the CROW's in Fig. 1 we can limit the mode expansion of Eq. (3) to the subspace spanned by these two degenerate modes $\mathcal{E}_l(\mathbf{r})$ with $l = \pm 1$, where the subscript l refers to the parity of the mode and can take only the value of ± 1. The degeneracy of the two modes gives $\Omega_l = \Omega$ for $l = \pm 1$. The symmetry of the modes also leads to $\alpha^1_{m,l}, \beta^1_{m,l}, \Delta\alpha_{m,l} = 0$ if $m \neq l$, which is obvious from Eq. (6). To further simplify Eq. (7), we also assume that the frequency difference between ω_K and Ω is small. Finally, the dispersion relations for the coupled-resonator modes are found to be

$$\omega^l_K = \Omega\left[1 - \frac{\Delta\alpha_{l,l}}{2} + \kappa_l \cos(KR)\right], \tag{9}$$

where l denotes the parity of the mode and the coupling coefficients κ_l are defined as

$$\begin{aligned}\kappa_l &= \beta^1_{l,l} - \alpha^1_{l,l} \\ &= \int \mathrm{d}\mathbf{r}[\epsilon_0(\mathbf{r} - R\mathbf{e}_x) - \epsilon(\mathbf{r} - R\mathbf{e}_x)]\mathcal{E}_l(\mathbf{r}) \\ &\quad \cdot \mathcal{E}_l(\mathbf{r} - R\mathbf{e}_x).\end{aligned} \tag{10}$$

For a given parity l, this dispersion relation defines a photonic band formed by coupling together the high-Q modes in the individual resonators with a definite parity, which we call the CROW band. These two CROW bands with $l = \pm 1$ have the same parity as those of the single-resonator modes. Therefore they can also be denoted as the even band and the odd band according to their parity.

From Eq. (9), the group velocity is found to be

$$v^l_g(K) = \frac{\mathrm{d}\omega^l_K}{\mathrm{d}K} = -\Omega R \kappa_l \sin(KR), \tag{11}$$

which we can make small by reducing the coupling coefficient κ_l. It is also interesting to observe that the dispersion and the group velocity of the two CROW bands, given in Eqs. (9) and (11), are exactly the same as the results of the nondegenerate analysis.[3] This is directly due to the fact that the two degenerate single-resonator modes have opposite parity and cannot couple to each other.

In the above analysis, the waveguide loss, which can be important in practice, is ignored. To take it into account, we introduce a lossy medium with absorption coefficient $\sigma(\mathbf{r})$ to simulate the free space surrounding the CROW. In this case, the waveguide modes of the CROW can be written as

$$\mathbf{E}_K(\mathbf{r}, t) = A\exp(-\Gamma_K t)\exp(i\omega_K t)\sum_{n,l} \times \exp(-inKR)\, b_l \mathcal{E}_l(\mathbf{r} - nR\mathbf{e}_x), \tag{12}$$

which satisfies

$$\nabla \times [\nabla \times \mathbf{E}_K] = -\frac{\epsilon(\mathbf{r})}{c^2}\frac{\partial^2 \mathbf{E}_K}{\partial t^2} - 4\pi\frac{\sigma(\mathbf{r})}{c^2}\frac{\partial \mathbf{E}_K}{\partial t}, \tag{13}$$

from which Γ_K is found to be

$$\Gamma_K = 2\pi\frac{\int \mathrm{d}\mathbf{r}\sigma(\mathbf{r})\mathbf{E}^*_K \cdot \mathbf{E}_K}{\int \mathrm{d}\mathbf{r}\epsilon(\mathbf{r})\mathbf{E}^*_K \cdot \mathbf{E}_K}. \tag{14}$$

A more useful expression for Γ_K will be given below. Here, it suffices to notice that generally Γ_K depends on K.

3. FDTD SIMULATION OF THE CROW

A. Numerical Algorithm

The FDTD method was proposed by Yee[13] in 1966. Since then it has been used extensively in computational electrodynamics. In this paper we use an iteration algorithm based on this FDTD method to calculate both the eigenmodes and the eigenfrequencies of a given dielectric structure. This algorithm is briefly summarized in this section. For more details the reader may consult Ref. 14, in which the FDTD method is extensively reviewed.

If we know the resonant frequency of a particular high-Q mode to be ω, the mode's spatial profile can be found simply by the following mode filtering technique. First, we temporally evolve the Maxwell equations

$$\frac{1}{c}\frac{\partial \mathbf{B}(\mathbf{r}, t)}{\partial t} = -\nabla \times \mathbf{E}(\mathbf{r}, t), \tag{15a}$$

$$\frac{\epsilon(\mathbf{r})}{c}\frac{\partial \mathbf{E}(\mathbf{r}, t)}{\partial t} = \nabla \times \mathbf{B}(\mathbf{r}, t) \tag{15b}$$

to find a time-varying electromagnetic field $\mathbf{E}(\mathbf{r}, t)$ and $\mathbf{B}(\mathbf{r}, t)$. This time-varying field generally contains a broad frequency spectrum, which depends on the choice of the initial field $\mathbf{E}(\mathbf{r}, 0)$ and $\mathbf{B}(\mathbf{r}, 0)$. By filtering the field $\mathbf{E}(\mathbf{r}, t)$ and $\mathbf{B}(\mathbf{r}, t)$, using a narrow-bandwidth frequency filter centered at ω, we find the electromagnetic mode at frequency ω. In our algorithm we achieve this mode filtering process simply by applying a temporal Fourier transformation at the given frequency ω to the above time-varying field:

$$\mathbf{E}(\mathbf{r}, \omega) = \int_0^T \mathrm{d}t\exp(-i\omega t)\,\mathbf{E}(\mathbf{r}, t), \tag{16a}$$

$$\mathbf{B}(\mathbf{r}, \omega) = \int_0^T \mathrm{d}t\exp(-i\omega t)\,\mathbf{B}(\mathbf{r}, t). \tag{16b}$$

The result, $\mathbf{E}(\mathbf{r}, \omega)$ and $\mathbf{B}(\mathbf{r}, \omega)$, is the high-$Q$ mode within the given dielectric structure $\epsilon(\mathbf{r})$ and has resonant frequency ω. It should be noted that mode $\mathbf{E}(\mathbf{r}, \omega)$ and $\mathbf{B}(\mathbf{r}, \omega)$ has a frequency uncertainty of the order $1/T$, because the temporal integration in Eqs. (16) has a frequency bandwidth of the order of $1/T$.

However, if we know only the spatial distribution of a high-Q mode to be $\mathbf{E}(\mathbf{r})$ and $\mathbf{B}(\mathbf{r})$, we can also find its resonant frequency ω by noticing that[9]

$$\nabla \times \left[\frac{1}{\epsilon(\mathbf{r})} \nabla \times \mathbf{B}(\mathbf{r}) \right] = \left(\frac{\omega}{c} \right)^2 \mathbf{B}(\mathbf{r}), \tag{17a}$$

$$\nabla \times [\nabla \times \mathbf{E}(\mathbf{r})] = \left(\frac{\omega}{c} \right)^2 \epsilon(\mathbf{r}) \mathbf{E}(\mathbf{r}). \tag{17b}$$

Consequently, resonant frequency ω and spatial distribution $\mathbf{E}(\mathbf{r})$ and $\mathbf{B}(\mathbf{r})$ of the given high-Q mode satisfy

$$\omega^2 = c^2 \frac{\int_V \mathrm{d}\mathbf{r} \left(\mathbf{B}^*(\mathbf{r}) \cdot \left\{ \nabla \times \left[\frac{1}{\epsilon(\mathbf{r})} \nabla \times \mathbf{B}(\mathbf{r}) \right] \right\} + \mathbf{E}^*(\mathbf{r}) \cdot \{ \nabla \times [\nabla \times \mathbf{E}(\mathbf{r})] \} \right)}{\int_V \mathrm{d}\mathbf{r} [\mathbf{B}^*(\mathbf{r}) \cdot \mathbf{B}(\mathbf{r}) + \epsilon(\mathbf{r}) \mathbf{E}^*(\mathbf{r}) \cdot \mathbf{E}(\mathbf{r})]}, \tag{18}$$

where the spatial integration is over the whole computational domain V.

Combining the mode filtering technique [Eqs. (16)] and the ability to find the resonant frequency of a given mode [Eq. (18)], we can iteratively find the high-Q mode of interest and its resonant frequency, starting from a good initial guess of field distribution $\mathcal{E}_0(\mathbf{r})$ and mode frequency Ω_0. First we evolve the guess field $\mathcal{E}_0(\mathbf{r})$, using Eqs. (15). Then, from Eqs. (16), we can filter out a mode $\mathcal{E}_1(\mathbf{r})$ from the time evolution of $\mathcal{E}_0(\mathbf{r})$, using the guess frequency Ω_0. Next, the average frequency Ω_1 of mode $\mathcal{E}_1(\mathbf{r})$ is obtained from Eq. (18). Subsequently, we can use $\mathcal{E}_1(\mathbf{r})$ and Ω_1 as the field distribution and the mode frequency and resume the iteration. This process is repeated until it converges and gives the desired high-Q mode. This iteration algorithm is also summarized in Fig. 2.

For the numerical calculations in this paper we consider only 2D structures, which can give a good approximation of the original three-dimensional problem if an appropriate effective refractive index is used.[26] In this paper we use an effective refractive index $n = 2.65$ for the dielectric medium to simulate a half-wavelength-thick slab waveguide with refractive index $n = 3.4$.[6] A major advantage of this 2D approximation is that it speeds up the numerical simulations and renders them more memory efficient. Our 2D computational domains are sketched in Fig. 3. The dielectric structure varies in the xy plane and remains the same along the third direction $\mathbf{e}_z$. Consequently k_z, the z component of the photon momentum, is conserved in this type of structure. Furthermore, under the condition that $k_z = 0$, the electromagnetic modes can be classified into TE modes and TM modes. The TE modes consist of only E_x, E_y, and B_z components, and TM modes have only E_z, B_x, and B_y components. In this paper we restrict ourselves to the TE modes. To achieve this goal, we use an initial field whose only nonzero component is the B_z component.

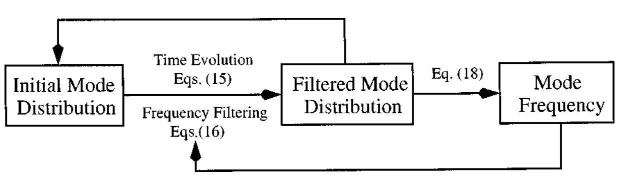

Fig. 2. FDTD algorithm to calculate the eigenmodes and the eigenfrequencies of a given dielectric structure.

To calculate the eigenmode and the eigenfrequency numerically, however, we still need to know how to terminate the computational domain by using appropriate boundary conditions. In fact, we use the same iteration process as summarized in Fig. 2 to analyze both the single resonators and the CROW's. The difference between the two cases lies in the boundary conditions, which are also sketched in Fig. 3. In Fig. 3(a) the boundary conditions for a single-defect cavity in a 2D photonic crystal are illustrated. For the bottom y boundary, we use the mirror boundary condition, which is implemented according to Eqs. (8). For all three other boundaries, the first-order Mur absorbing boundary[27] is used to simulate the free space surrounding the optical resonator. The boundary conditions for the CROW composed of coupled defect cavities are shown in Fig. 3(b). For the top y boundary, we use the quartic perfectly matched layer[28,29] (PML) boundary to absorb the incident electromagnetic waves and simulate free space. Here we use the PML boundary condition because it is superior to the Mur boundary condition and can achieve a much lower reflectivity,[28,29] which is critical in the simulation of the CROW's. For the bottom y boundary we use the same mirror boundary condition as in the single-resonator case. For the two x boundaries, $x = 0$ and $x = R$, the Bloch boundary condition is used:

$$\mathbf{E}(x = R, y) = \exp(-iKR)\, \mathbf{E}(x = 0,\, y), \tag{19a}$$

$$\mathbf{B}(x = R, y) = \exp(-iKR)\, \mathbf{B}(x = 0,\, y), \tag{19b}$$

where K represents the crystal momentum of the CROW band. This Bloch boundary condition allows us to reduce the infinite CROW to a single unit cell and makes the numerical simulation possible. Varying K from $-\pi/R$ to π/R, we can use the above iteration process to find the eigenmodes and the eigenfrequencies throughout the entire CROW band.

To evaluate the quality factor of a single-resonator mode, we use the definition

$$Q = \frac{E_{\mathrm{mode}}^{\mathrm{avg}}}{E_{\mathrm{mode}}(0) - E_{\mathrm{mode}}(T)} \Omega_{\mathrm{mode}} T, \tag{20}$$

where $E_{\mathrm{mode}}(T)$ is the total energy of that mode at time T (the end of evolution), $E_{\mathrm{mode}}(0)$ is the mode energy at time

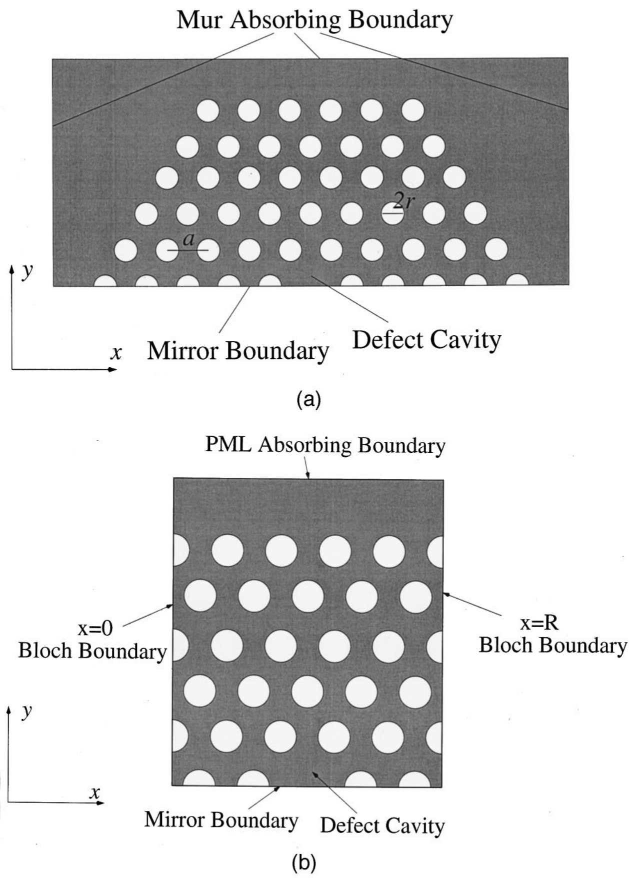

Fig. 3. FDTD computational domain. (a) For the calculation of a single defect cavity in a 2D photonic crystal. The photonic crystal is characterized by a, the distance between the nearest air holes, and r, the radius of the air hole. The mirror boundary condition is used at the bottom y boundary. For the other three boundaries the first-order Mur absorbing boundary is used. (b) For the calculation of CROW composed of coupled defect cavities with four air holes between them. The PML absorbing boundary condition and the mirror boundary condition, respectively, are used for the top and bottom y boundaries. At both of the x boundaries, $x = 0$ and $x = R$, the Bloch boundary condition is used.

0 (the beginning of evolution), $E_{\mathrm{mode}}^{\mathrm{avg}}$ is the average mode energy during the time evolution, and Ω_{mode} is the frequency of the mode.

For the case of the CROW, we can define an effective quality factor $Q_{\mathrm{eff}}(K)$ as

$$Q_{\mathrm{eff}}(K) = \frac{\omega_K}{2\Gamma_K}, \tag{21}$$

where Γ_K is defined in Eq. (12). The physical meaning of this effective Q can be clarified from the following considerations: We have known that the photons stored in the individual resonator of the CROW can propagate by hopping into the neighbor resonators.[3] However, they can also leak out of the CROW and therefore cause the CROW modes to decay. Consequently, it is clear that this $Q_{\mathrm{eff}}(K)$ is similar to the Q factor of single-resonator cavities and characterizes the rate at which the photons in each individual resonator leak out of the CROW. $Q_{\mathrm{eff}}(K)$ can also be calculated by use of Eq. (20) in the same way as the Q factor of the single resonator.

The decay of the modes leads to an uncertainty of the mode resonant frequency, which is the dominant source of the frequency errors in our simulations. Consider a mode with a mode frequency Ω and quality factor (or effective quality factor) Q. In as much as the mode evolves temporally according to $\exp[(-1/2Q+i)\Omega t]$, the calculated mode frequency will bear an uncertainty of order $\Omega/2Q$.

In all the numerical calculations in this paper we have normalized c to 1, which means that length and time have the same unit. We have also set the spatial increment in the x and y directions, the size of FDTD cells, to be 1. It should also be noted that all the wavelengths λ that appear in the remainder of this paper refer to wavelengths in free space.

B. Coupled Defect-Cavity Waveguide

The 2D single defect cavity formed by plugging an air hole from the 2D triangular lattice photonic crystal is illustrated in Fig. 3(a). The properties of this 2D triangular lattice photonic crystal are determined by the ratio r/a, where r is the radius of the air hole and a is the interhole distance. In all the calculations of this section, we choose $a = 15$ and $r/a = 0.3$ and use a/λ as the unit of frequency.

The 2D photonic crystal with $r/a = 0.3$ has a bandgap for TE modes in a frequency range of a/λ from 0.28 to 0.35.[6] Within this TE bandgap, the single defect cavity can support two degenerate high-Q modes. The two modes, classified according to the mirror reflection symmetry, possess opposite parities with respect to the lower y boundary in Fig. 3(a). The mode with $P = 1$ is called the even defect mode, and that with $P = -1$ is called the odd defect mode. These two modes are numerically calculated, and the results are shown in Fig. 4. The field distribution in Fig. 4 is that of the B_z component. (In fact, all the figures of mode spatial profile in this paper

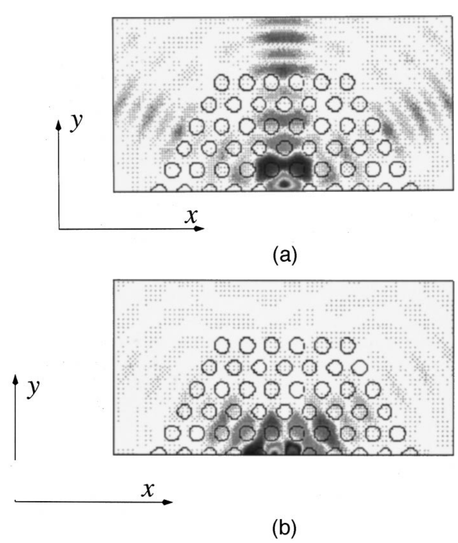

Fig. 4. High-Q modes of a single defect cavity surrounded by five layers of air holes. Even and odd single defect modes are shown in (a) and (b), respectively.

show the B_z component.) However, because the **B** field transforms as a pseudovector under mirror reflection, the B_z field of the even defect mode actually is antisymmetric with respect to the lower y boundary, as in Fig. 4(a). For the same reason, the B_z field of the odd defect mode is actually symmetric with respect to the lower y boundary. The frequency and the Q factor of the even mode are, respectively, 0.301 and 840, whereas the frequency and the Q factor of the odd mode are 0.310 and 780. The degeneracy of the two modes is broken because the air holes in the numerical simulation are not ideally circular; another possible reason is the presence of the absorbing boundaries, which also break the symmetries of the single-defect cavity. It should be emphasized that this degeneracy splitting has no significant influence on the CROW mode characteristics, because the two defect cavity modes still possess opposite parity and remain orthonormal to each other. As is clear from the analysis leading to Eq. (9), each of the two CROW bands remains independent of the other and can still be characterized by a single coupling coefficient κ_l.

Using the algorithm in Subsection 3.A, we study three cases for this type of CROW, with spacings between adjacent defect cavities of two, three, and four holes, respectively. In Fig. 3(b) we sketch the FDTD computational domain for the CROW with intercavity spacing of four air holes. To map out the CROW band, we increase the crystal momentum K from 0 to π/R in increments of $0.1\pi/R$. Because of symmetry considerations, the CROW bands are symmetric with respect to the $K = 0$ axis. Therefore it is sufficient for us to concentrate on the half with $K \geqslant 0$.

First we consider the even CROW bands. In Fig. 5 we show two waveguide modes with intercavity spacing of two and four air holes and $K = 0.6\pi/R$. Comparing Fig. 5 with Fig. 4(a), we can clearly see that the waveguide modes in the CROW closely resemble the single-resonator mode. As expected from the tight-binding analysis, this similarity is not restricted to this particular K value and holds through all the CROW bands.

The dispersion curves for the even CROW bands are shown in Fig. 6. Using the least-squares method,[30] we fit the calculated frequency versus K to Eq. (9) and obtain three coupling coefficients κ_1. For intercavity spacing of two, three, and four holes, κ_1 is, respectively, 5.6×10^{-3}, -1.4×10^{-3}, and -2.9×10^{-4}. It is obvious from Fig. 6 that the coupling coefficient decreases with the intercavity distance and changes sign for the CROW band with three-hole spacing. Such results can be understood as follows: From Eq. (10), we know that the coupling coefficient is an overlap integral of two single-defect cavity modes with a distance of R between them. As the evanescent field of the single-resonator mode decays oscillationally, this overlap integral will also decrease oscillationally as a function of R. The effective Q of the even CROW band is also calculated and found to be close to the value of 1500 throughout the CROW bands.

Next we analyze the odd CROW band and, as before, use three different intercavity spacings: two holes, three holes, and four holes. In Fig. 7 we show the waveguide modes with $K = 0.6\pi/R$ and three-air-hole spacing. This CROW mode is qualitatively the same as the odd de-

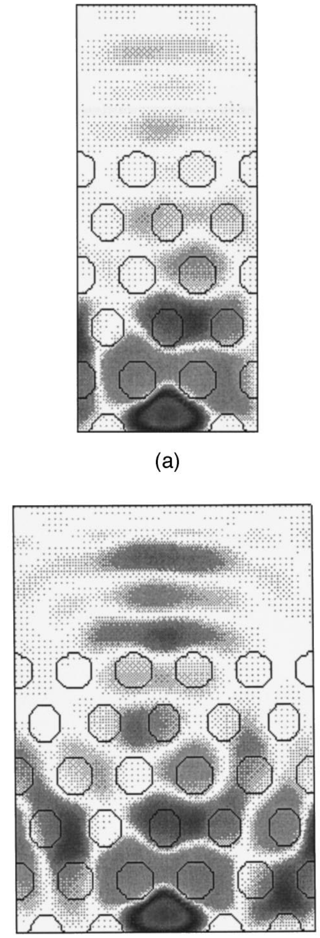
(a)

(b)

Fig. 5. Even waveguide modes of the CROW with different intercavity hole spacings. The spacing is two holes in (a) and four holes in (b). The crystal momentum K of both the waveguide modes is $K = 0.6\pi/R$.

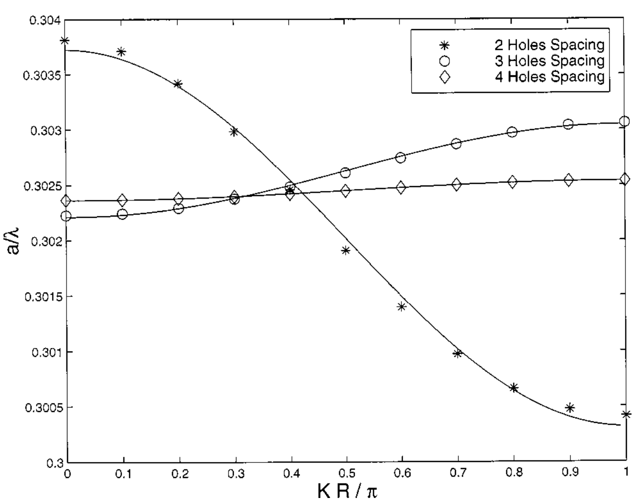

Fig. 6. Dispersion diagram of the even CROW band of coupled defect cavities. The frequencies, calculated with the FDTD algorithm, are shown for intercavity spacings of two, three and four air holes. Solid curves are least-squares fits of the numerical results with Eq. (9).

fect mode in Fig. 4(b). As before, this similarity holds through all the CROW bands.

The dispersion relations of the odd CROW modes are shown in Fig. 8. We then fit the numerical calculated mode frequency as a function of K into Eq. (9), using the least-squares method. From this fitting, the coupling coefficients κ_{-1} are found to be, respectively, 1.24×10^{-2}, 4.5×10^{-3}, and 1.7×10^{-3} for spacings of two, three, and four holes. Again as expected, the coupling decreases as the intercavity spacing increases. It should also be noticed that the coupling coefficients of the odd CROW modes are larger than those of the even CROW modes with the same hole spacing. This is so because the even defect mode radiates more strongly along the $\mathbf{e}_y$ direction than the $\mathbf{e}_x$ direction, whereas the opposite holds true for the odd defect mode, as can be seen from Fig. 4. Another consequence of this fact is that the effective Q of the odd CROW modes should be much larger than that of the corresponding even CROW modes, which is also confirmed by our numerical calculations and is obvious by comparison of Figs. 5 and 7. In fact, all the Q_{eff} of the odd CROW modes are found to be larger than 10^6. Unfortunately, these results are only qualitatively correct, because a precise calculation of the Q factor requires a time evolution of the order of Q optical periods, which is impractical for Q factors large as those.

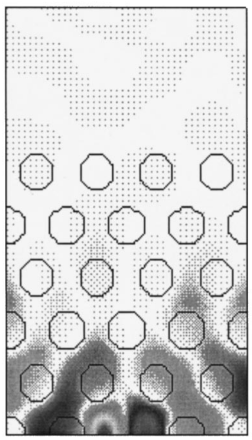

Fig. 7. Odd waveguide mode of the CROW with intercavity hole spacing of three air holes. The crystal momentum K of the waveguide mode is $0.6\pi/R$.

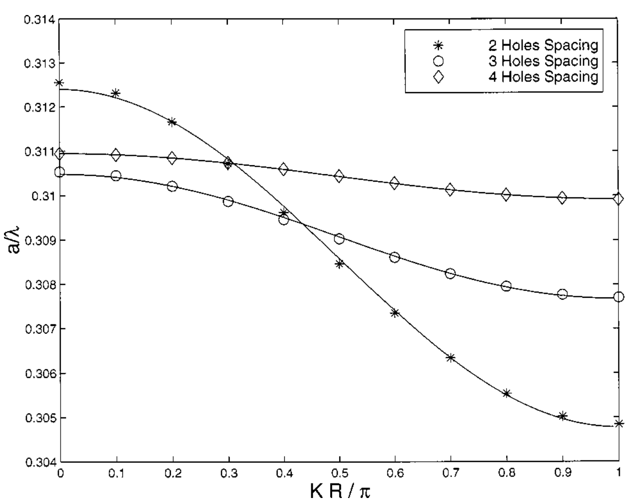

Fig. 8. Dispersion diagram of the odd CROW band of coupled defect cavities. The frequencies, calculated with FDTD algorithm, are shown for intercavity spacings of two, three and four air holes. Solid curves are least-squares fits of the numerical results with Eq. (9).

We also calculate the coupling coefficient by using the overlap integral in Eq. (10). We choose $\epsilon_0(\mathbf{r})$ to be a single-defect cavity surrounded by five layers of air holes in the $\mathbf{e}_y$ direction and nine layers of air holes in the $\mathbf{e}_x$ direction. Then we calculate the even and odd defect modes of such a single-defect cavity and use them to obtain κ_1 and κ_{-1}. They are shown in Table 1, together with the coupling coefficients from least-squares fitting. The results for relatively large κ_1 agree well with those obtained from least-squares fitting. However, the deviation is larger for κ_{-1}. For both κ_1 and κ_{-1}, as the coupling between the individual resonators becomes weaker, the discrepancy between the tight-binding results and the FDTD results is more pronounced. The difference between these two results, we believe, is likely caused by the fact that we assume that the single-resonator mode $\mathcal{E}_l(\mathbf{r})$ is a real function [see Eq. (2)], which holds only when the loss of the cavity mode can be ignored. However, as the distance between the neighboring resonators becomes larger, the mode radiation loss, even though it is relatively small, will introduce a phase shift to the electromagnetic field that can no longer be ignored. This fact also helps to explain why the tight-binding results for κ_1 agree better with the FDTD results than in the case of κ_{-1}. Previously we showed that the even defect cavity mode radiates primarily along the $\mathbf{e}_y$ direction; therefore the phase shift in the $\mathbf{e}_x$ direction is relatively small. However, the odd cavity mode radiates more strongly along the $\mathbf{e}_x$ direction, which inevitably introduces a larger phase shift. In this case, assuming that the mode function are real causes larger deviations between the tight-binding results and the FDTD results.

We find that the CROW modes retain almost the same symmetry properties as the single defect-cavity modes throughout the whole CROW band. Using symmetry

Table 1. Coupling Coefficient κ_l of the Coupled Defect Cavities

	Coupling Coefficient κ_1			Coupling Coefficient κ_{-1}		
Number of holes[a]	2	3	4	2	3	4
Numerical result[b]	5.6×10^{-3}	-1.4×10^{-3}	-2.9×10^{-4}	1.24×10^{-2}	4.5×10^{-3}	1.7×10^{-3}
Theoretical result[c]	5.4×10^{-3}	-1.3×10^{-3}	1.7×10^{-4}	7.3×10^{-3}	7.0×10^{-4}	-9.0×10^{-4}

[a] Number of air holes between the adjacent defect cavities.
[b] Obtained from fitting the dispersion relation by use of Eq. (9).
[c] Obtained from the overlap integral in Eq. (10).

considerations similar to those of Ref. 31, we can use this unique property of the CROW to construct waveguides without crosstalk, as shown in Fig. 9. Suppose that there are two branches of CROW's. The one along the $\mathbf{e}_x$ direction is called the X branch, and the corresponding single-resonator modes are called X modes. The other branch, along the $\mathbf{e}_y$ direction, is called the Y branch, and the single-resonator modes are called Y modes. Assume that the two branches are joined at the 0th resonator. From Fig. 9 it is clear that, if the overlap integral between the X and the Y modes is zero, the X mode in the 0th resonator cannot excite the Y mode that propagates along the $\mathbf{e}_y$ direction and vice versa. If, within a certain frequency range, the CROW supports only these two types of waveguide mode, then the crosstalk between the two branches of CROW's can be eliminated. In Fig. 9 the X modes are symmetric with respect to the yz mirror plane and antisymmetric with respect to the xz mirror plane. The Y modes have exactly the opposite symmetry properties. Consequently, the overlap integral between the two modes is zero and satisfies our condition for waveguiding without crosstalk.

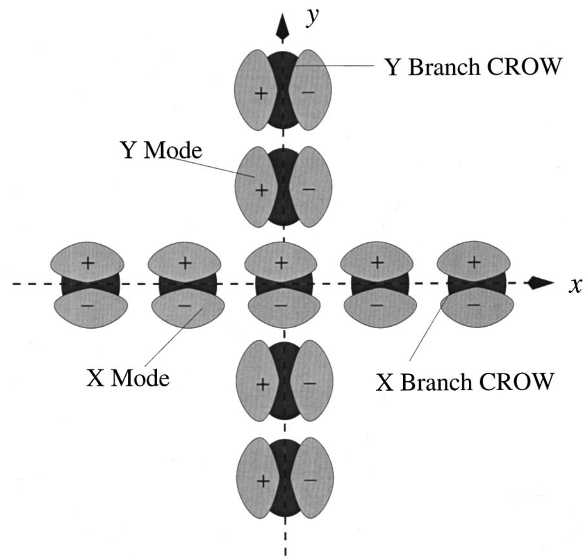

Fig. 9. CROW intersection without cross talk. The CROW's contain two branches, an X branch and a Y branch. The darker shaded regions refer to the single resonators that compose the CROW's. Two types of single resonator mode, an X mode and a Y mode, are supported by the X branch and the Y branch, respectively, represented by the lighter shaded regions. The X mode is antisymmetric with respect to the xz plane and symmetric with respect to the yz plane. The Y mode has exactly the opposite symmetry properties.

C. Coupled-Microdisk Waveguide

It is well known that a dielectric microdisk cavity can support high-Q whispering-gallery modes, which can be classified according to their polarization (TE or TM), their azimuthal mode number m, and their radial mode number l.[10,11] A TE whispering-gallery mode TE(m, l) has $2m$ nodes in the azimuthal direction and $l - 1$ nodes in the radial direction. It is also doubly degenerate and can be classified as an even or an odd mode according to its mirror reflection symmetry. By coupling the microdisks together as in Fig. 1(b), we can form the even and odd CROW bands from such whispering-gallery modes. In this section we study the CROW bands formed by the TE$(7, 1)$ whispering-gallery modes.

In these calculations, we choose the radius r of the microdisk to be 30 FDTD cells and use three parameters for the intermicrodisk spacing R, which is normalized as $R/2r$ and takes the values $R/2r = 1.1, 1.17, 1.23$. r/λ is used as the unit of frequency.

The TE$(7, 1)$ even mode and odd mode of a single microdisk are shown in Fig. 10. The frequency and the Q factor of the even TE$(7, 1)$ mode are found to be 0.645 and 1500. For the odd TE$(7, 1)$ mode, the frequency and the Q factor are 0.639 and 1200, respectively. The degeneracy of the two TE$(7, 1)$ modes is broken as a result of the deviation of the dielectric microdisk from an ideal circular shape in our 2D simulation. As in the case of photonic crystal defect cavities, such degeneracy splitting will not cause significant changes in the dispersion and mode characteristics of the CROW band because the even and odd CROW modes remain orthonormal to each other.

Using the algorithm described in Subsection 3.A, we calculate the even CROW bands for three microdisk spacing parameters $R/2r$. Shown in Fig. 11 is the mode profile of a waveguide mode with $R/2r = 1.1$ and $K = 0.5\pi/R$. It is qualitatively the same as that of the even TE$(7, 1)$ mode in Fig. 10(a). This suggests that the tight-binding approximation is still valid, even for the close coupling of our microdisks.

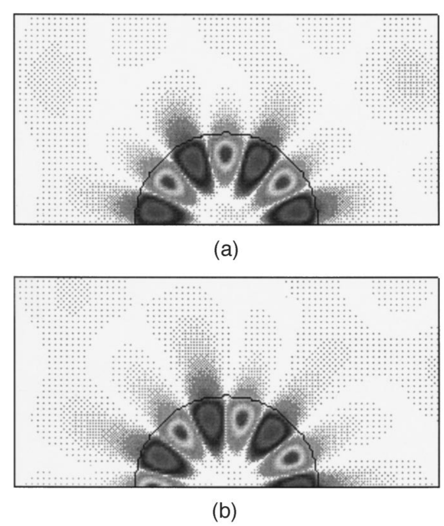

Fig. 10. TE$(7, 1)$ whispering-gallery modes in a single microdisk cavity. The mode with even mirror reflection symmetry is shown in (a), and the one with odd mirror reflection symmetry is shown in (b).

The effective Q of the even CROW bands is found to depend strongly on the crystal momentum K. $Q_{\mathrm{eff}}(K)$ of the CROW band with $R/2r = 1.17$ is shown in Fig. 12 as a function of K. The fact that effective Q depends on K is not surprising, as can be expected from Eq. (14). However, it can also be explained in a more intuitive way. The TE(m, l) mode has an azimuthal dependence of $\exp(im\phi)$,[10,11] which means that its radiation loss has similar angular dependence. When K, the crystal momentum of the CROW modes varies, the radiation fields from different individual resonators interfere constructively or destructively with each other, which consequently causes the radiation loss of the CROW modes to increase or decrease and to deviate from that of the single microdisk resonator.

The dispersion relations for the even CROW modes with three different values of $R/2r$ are shown in Fig. 13. The error bars in Fig. 13 refer to the frequency uncertainty that is due to the radiation decay of the CROW modes, which is estimated to be $\omega_K/2Q_{\mathrm{eff}}$ as in Subsection 3.A. Within the limit of these frequency errors, the numerical data agree well with the tight-binding results.

These frequency errors are also taken into account when we fit the numerical results into Eq. (9), using the least-squares method. We no longer treat the numerically calculated mode frequencies equally and weigh them by the frequency deviation of $\omega_K/2Q_{\mathrm{eff}}$. The coupling coefficients κ_1 obtained from this fitting are, respectively, -4.5×10^{-3}, -2.5×10^{-3}, and -1.3×10^{-3} for values of $R/2r = 1.1, 1.17, 1.23$. As expected, κ_1 decreases as the intermicrodisk spacing increases.

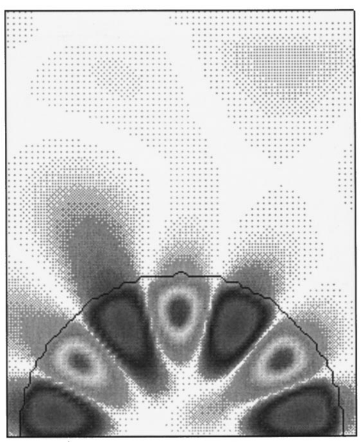

Fig. 11. Even waveguide mode of coupled microdisks, which is formed by coupling of the even TE(7, 1) modes together. $R/2r$, the ratio of intermicrodisk spacing to the microdisk diameter, is 1.1, and $K = 0.5\pi/R$.

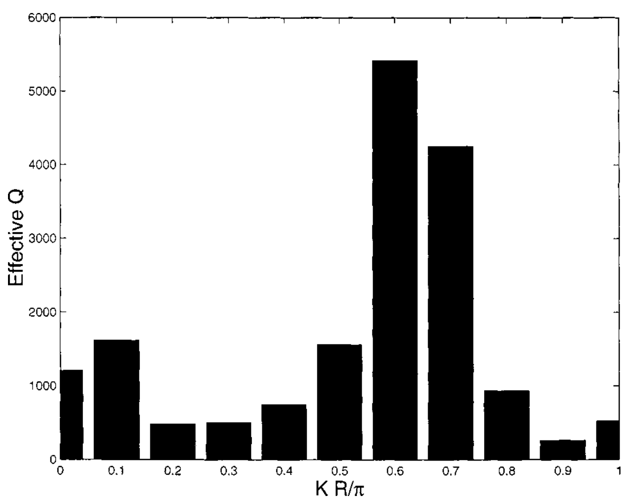

Fig. 12. Effective Q factors of the even CROW modes of the coupled microdisks for parameter $R/2r = 1.17$. Q_{eff} is calculated according to Eq. (20).

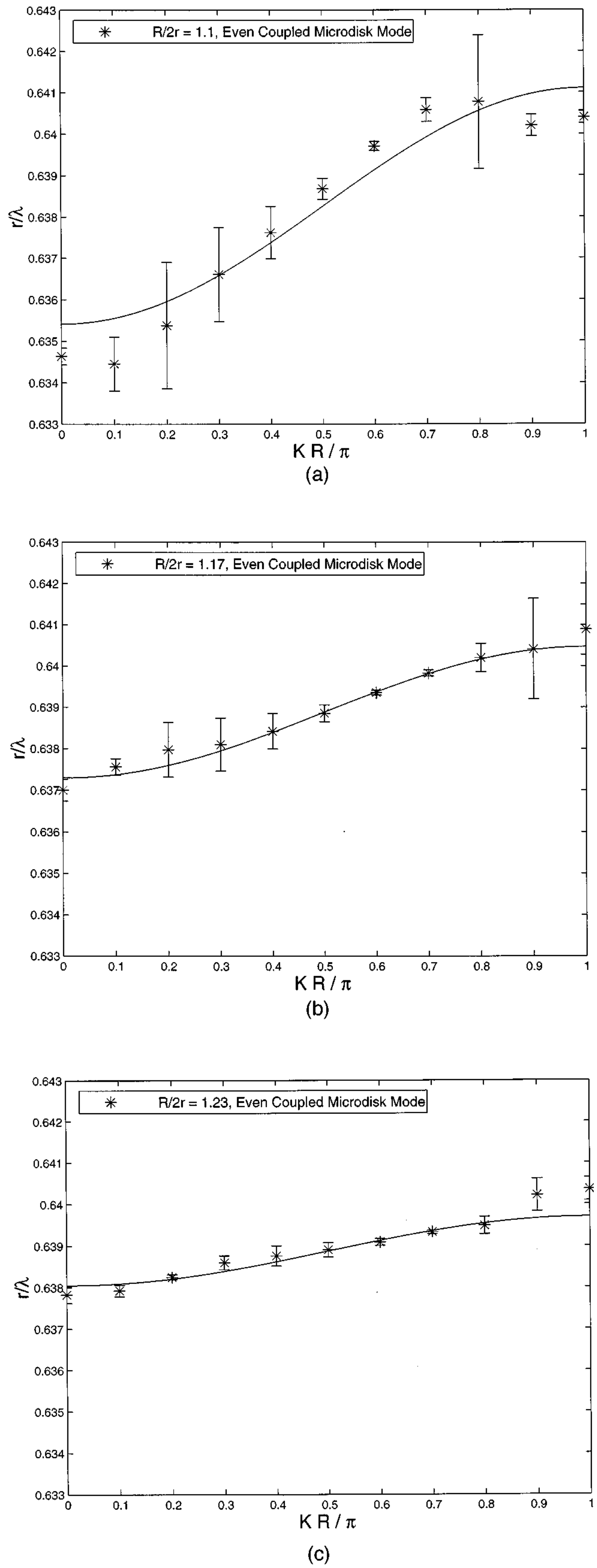

Fig. 13. Dispersion relations of the even CROW band of coupled microdisks. The numerically calculated results are represented by asterisks. The error bars refer to the frequency error caused by the finite decay rate of the CROW modes and are estimated to be $\omega/2Q_{\mathrm{eff}}$. Solid curves are least-squares fits of the numerical results with Eq. (9).

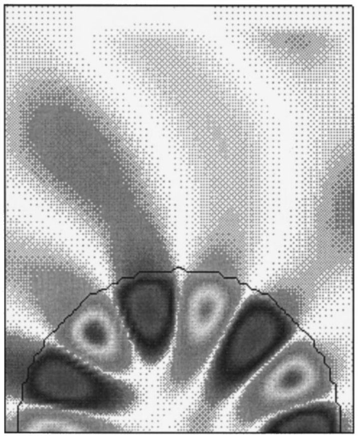

Fig. 14. Odd waveguide mode of coupled microdisks, which is formed by coupling of the odd TE(7, 1) modes together. $R/2r$, the ratio of intermicrodisk spacing to the microdisk diameter, is 1.1, and $K = 0.5\pi/R$.

We calculate the odd CROW bands, using the same set of values for $R/2r$. The CROW mode shown in Fig. 14 is calculated with $R/2r = 1.1$ and $K = 0.5\pi/R$ and, as before, is similar to the odd TE(7, 1) mode shown in Fig. 10(b). The odd CROW bands are shown in Fig. 15 for $R/2r = 1.1, 1.17, 1.23$. Again, after the frequency deviation that is due to the decay of CROW modes is considered, the numerical results agree well with the theoretical fits. The results for κ_{-1} obtained from the theoretical fitting are, respectively, 4.8×10^{-3}, 2.9×10^{-3}, and 1.4×10^{-3} for $R/2r = 1.1, 1.17, 1.23$.

In the case of coupled microdisks it is difficult to calculate the coupling coefficient by using the overlap integral in Eq. (10). One reason is that the electromagnetic field outside the microdisk depends strongly on the boundary conditions of the computational domain, especially in the regions far from the microdisk. This is quite different from the case of the defect cavity in the 2D photonic crystal, for which the photonic crystal can effectively block much of the influence of the absorbing boundaries. Another reason is that the electromagnetic field does not decay exponentially away from the microdisk and therefore creates a normalization problem.

4. SHG IN THE CROW

In Ref. 3, the argument that for a given input optical power the electric field strength is inversely proportional to the group velocity of a photonic band showed that the CROW's can be used to greatly enhance the efficiency of nonlinear optical processes. Here we analyze in detail the SHG process in the CROW. This analysis, however, is not limited by the tight-binding approximation of the CROW and in principle can be applied to any dielectric structures with one-dimensional discrete translational symmetry.

Using the Bloch theorem, we can express the waveguide mode of a CROW in terms of a periodic Bloch wave function. Assume that the waveguide is periodic in the x direction with a spatial period R (see Fig. 1 for an example); the waveguide mode $\mathbf{E}_K(\mathbf{r}, t)$ can be written as

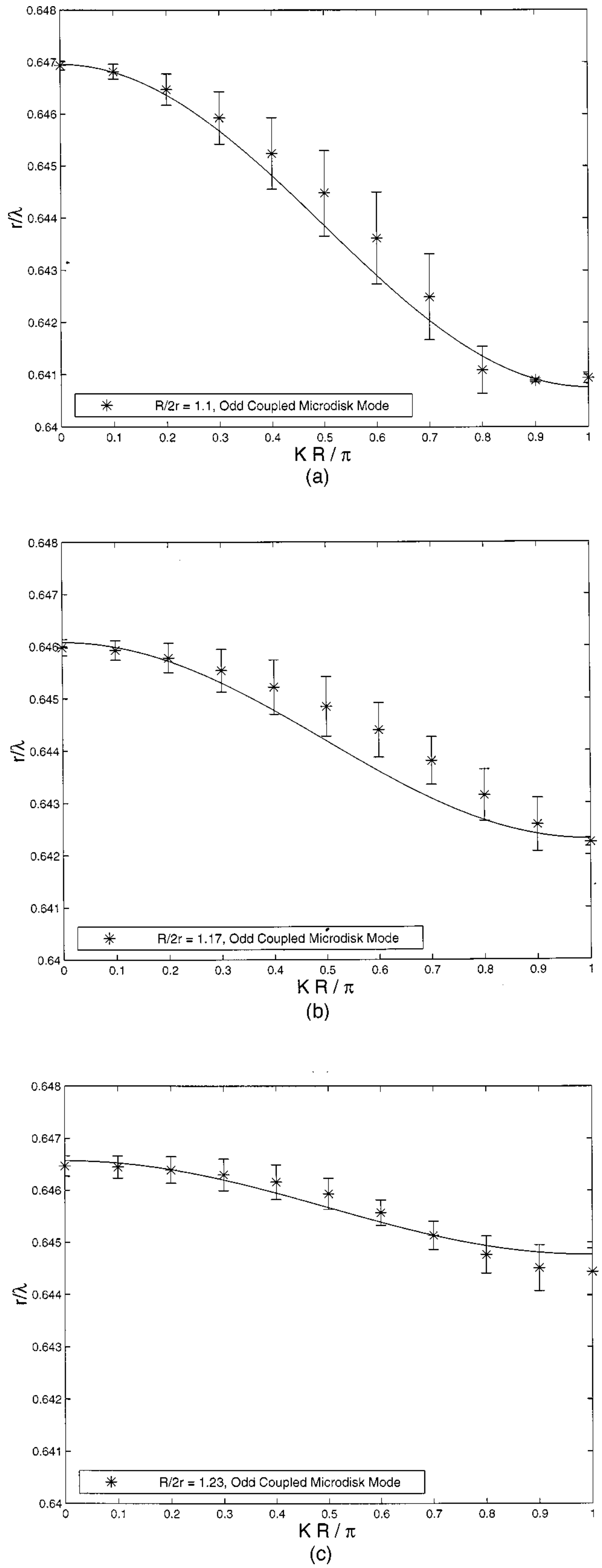

Fig. 15. Dispersion relations of the odd CROW band of coupled microdisks. The numerically calculated results are represented by asterisks. The error bars refer to the frequency error caused by the finite decay rate of the CROW modes and are estimated to be $\omega/2Q_{\mathrm{eff}}$. Solid curves are least-squares fits of the numerical results with Eq. (9).

$$\mathbf{E}_K(r,\ t) = \exp[(-\Gamma_\omega + i\omega)t]\exp(-iK\mathbf{e}_x \cdot \mathbf{r})\mathbf{u}_K(\mathbf{r}), \quad (22)$$

where the Bloch wave function $\mathbf{u}_K(\mathbf{r})$ is periodic, $\mathbf{u}_K(\mathbf{r} + R\mathbf{e}_x) = \mathbf{u}_K(\mathbf{r})$, and normalized within a unit cell: $\int_{\mathrm{uc}} \mathrm{d}\mathbf{r}\epsilon(\mathbf{r})\mathbf{u}_K^*(\mathbf{r}) \cdot \mathbf{u}_K(\mathbf{r}) = 1$. The frequency and the decay rate of this mode are represented by ω and Γ_ω, respectively.

Waveguide mode $\mathbf{E}_K(\mathbf{r},\ t)$ satisfies

$$\nabla \times [\nabla \times \mathbf{E}_K] + \frac{4\pi}{c^2}\sigma(\mathbf{r})\frac{\partial \mathbf{E}_K}{\partial t} = -\frac{\epsilon(\mathbf{r})}{c^2}\frac{\partial^2 \mathbf{E}_K}{\partial t^2}, \quad (23)$$

where $\sigma(\mathbf{r})$ is introduced to account for the radiation loss of the waveguide mode. By substituting Eq. (22) into Eq. (23) we can separate wave equation (23) into an imaginary part and a real part. From the imaginary part we can derive an expression for the mode decay rate Γ_ω:

$$\Gamma_\omega = 2\pi \int_{\mathrm{uc}} \mathrm{d}\mathbf{r}\sigma(\mathbf{r})\mathbf{u}_K^*(\mathbf{r}) \cdot \mathbf{u}_K(\mathbf{r}). \quad (24)$$

From the real part an eigenequation for Bloch wave function $\mathbf{u}_K$ can be derived, from which we express the the group velocity of a particular photonic band as

$$v_{\omega,g} = \frac{c^2}{2\omega}\int_{\mathrm{uc}} \mathrm{d}\mathbf{r}\mathbf{u}_K^* \cdot \{-2K\mathbf{e}_x \times [\mathbf{e}_x \times \mathbf{u}_K] - i\mathbf{e}_x \times [\nabla \times \mathbf{u}_K] - i\nabla \times [\mathbf{e}_x \times \mathbf{u}_K]\}. \quad (25)$$

The derivation is given in Appendix A.

Having found the mode decay rate and the group velocity, we can proceed to analyze the SHG in the CROW. First let us limit our consideration to an electromagnetic field with three components: two fundamental frequency modes $\mathbf{E}_1(\mathbf{r},\ t)$ and $\mathbf{E}_1'(\mathbf{r},\ t)$ and a second harmonic mode $\mathbf{E}_2(\mathbf{r},\ t)$:

$$\mathbf{E}_1(\mathbf{r},\ t) = 1/2\{E_1 \exp(i\omega t)\exp[-iK_1(\omega)x]\mathbf{u}_{K_1}(\omega)(\mathbf{r}) + \mathrm{c.c.}\}, \quad (26a)$$

$$\mathbf{E}_1'(\mathbf{r},\ t) = 1/2\{E_1 \exp(i\omega t)\exp[-iK_2(\omega)x]\mathbf{u}_{K_{2(\omega)}}(\mathbf{r}) + \mathrm{c.c.}\}, \quad (26b)$$

$$\mathbf{E}_2(\mathbf{r},\ t) = 1/2\{E_2(x)\exp(i2\omega t)\exp[-iK(2\omega)x]\mathbf{u}_{K(2\omega)}(\mathbf{r}) + \mathrm{c.c.}\}. \quad (26c)$$

For simplicity, we assume that the two fundamental frequency modes have the same amplitude E_1 throughout the region of SHG (undepleted pump)[32] and also require the amplitude of the second-harmonic mode $E_2(x)$ to be a slowly varying function.

The second-harmonic mode is generated according to the following equation:

$$\nabla \times [\nabla \times \mathbf{E}_2] + \frac{4\pi}{c^2}\sigma(\mathbf{r})\frac{\partial \mathbf{E}_2}{\partial t} + \frac{\epsilon(\mathbf{r})}{c^2}\frac{\partial^2 \mathbf{E}_2}{\partial t^2} = -\frac{1}{c^2}\frac{\partial^2}{\partial t^2}\mathbf{P}_{\mathrm{NL}}(\mathbf{r},\ t). \quad (27)$$

The nonlinear polarization term $\mathbf{P}_{\mathrm{NL}}(\mathbf{r},\ t)$, the source of the second-harmonic mode, is given by[32]

$$\mathbf{P}_{\mathrm{NL}}(\mathbf{r},\ t) = \frac{1}{2}(E_1^2 \exp(i2\omega t)\exp\{-i[K_1(\omega)+K_2(\omega)]x\} \times \tilde{d}_{2\omega}(\mathbf{r})\mathbf{u}_{K_{1(\omega)}}(\mathbf{r})\mathbf{u}_{K_{2(\omega)}}(\mathbf{r}) + \mathrm{c.c.}), \quad (28)$$

where the tensor $\tilde{d}(\mathbf{r})$ represents the second-order nonlinear coefficient of the dielectric medium. Multiplying Eq. (27) from the left by $\mathbf{u}_{K(2\omega)}^*(\mathbf{r})$ and integrating spatially within a unit cell, after a long but straightforward derivation we obtain an equation for $E_2(x)$:

$$v_{2\omega,g}\frac{\mathrm{d}E_2(x)}{\mathrm{d}x} + \Gamma_{2\omega}E_2(x) = -i\omega E_1^2 \int_{\mathrm{uc}} \mathrm{d}\mathbf{r}\exp\{-i[K_1(\omega) + K_2(\omega) - K(2\omega)]x\} \times \mathbf{u}_{K(2\omega)}^* \cdot \tilde{d}\mathbf{u}_{K_{1(\omega)}}\mathbf{u}_{K_{2(\omega)}}, \quad (29)$$

where $v_{2\omega,g}$ is the group velocity of the second-harmonic mode and $\Gamma_{2\omega}$ is the corresponding decay rate. It is clear that $E_2(x)$ will always be small unless there exists an integer n such that the difference of the crystal momentum $K_1(\omega) + K_2(\omega) - K(2\omega) + n2\pi/R$ becomes very small. In such a case, Eq. (29) is simplified as

$$v_{2\omega,g}\frac{\mathrm{d}E_2(x)}{\mathrm{d}x} + \Gamma_{2\omega}E_2(x) = -i\omega D_n E_1^2 \exp(-i\Delta K_n x), \quad (30a)$$

$$\Delta K_n = K_1(\omega) + K_2(\omega) - K(2\omega) + n\frac{2\pi}{R}, \quad n = 0, \pm 1, \pm 2 \ldots, \quad (30b)$$

$$D_n = \int_{\mathrm{uc}} \mathrm{d}\mathbf{r}\exp[in(2\pi/R)x]\mathbf{u}_{K(2\omega)}^*(\mathbf{r}) \cdot \tilde{d}(\mathbf{r}) \times \mathbf{u}_{K_{1(\omega)}}(\mathbf{r})\mathbf{u}_{K_{2(\omega)}}(\mathbf{r}). \quad (30c)$$

According to Eqs. (30), a large E_2 is possible only under the condition that $\Delta K_n = 0$, which is the phase-matching condition in the CROW:

$$K(2\omega) = K_1(\omega) + K_2(\omega) + n\frac{2\pi}{R}, \quad n = 0, \pm 1, \pm 2 \ldots. \quad (31)$$

This phase-matching condition in the CROW is similar to that in the bulk medium, except for the appearance of the Bloch wave vector $n2\pi/R$.[15–19] This additional term $n2\pi/R$ is to be expected, because only the crystal momentum, instead of the true photon momentum, is conserved in the CROW.

Equations (30) are our master equations for the analysis of SHG. As an example, we use them to study two cases of phase-matched SHG configurations in a CROW. Unlike the previous 2D cases, here we consider a three-dimensional geometry as sketched in Fig. 16. This CROW is still composed of defect cavities in a 2D triangular lattice photonic crystal. But instead of being infinite in the third direction, it is confined in a slab wave-

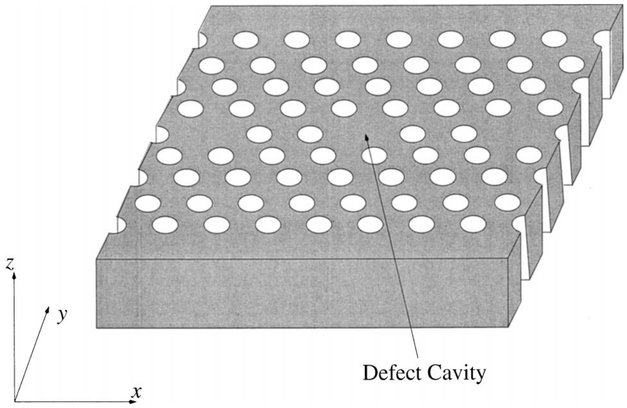

Fig. 16. SHG in the CROW. The fundamental frequency modes can propagate by hopping from one defect cavity to another along the x axis. The second-harmonic mode can either propagate in the CROW along the x axis or leak out of the CROW along the z axis.

guide along the z axis. The photon confinement is provided by the 2D photonic crystal in the xy plane and by total internal reflection in the z direction.[6]

In the first case, we assume that both of the fundamental frequency modes propagate along the positive x direction and satisfy $K_1(\omega) = K_2(\omega) = K(\omega)$ and $K(2\omega) = 2K(\omega)$. The second-harmonic photons also propagate along the x axis but can be collected either along the x direction or after leaking out along the z direction. We call this case SHG configuration I.

Assuming that the CROW begins at $x = 0$, we can require that $E_2(0) = 0$. From Eqs. (30), $E_2(x)$ is found to be

$$E_2(x) = -i\frac{\omega E_1^2 D_0}{\Gamma_{2\omega}}[1 - \exp(-\Gamma_{2\omega} x/v_{2\omega,g})]. \quad (32)$$

From this relation it is obvious that the SHG process has two distinctive limits, with $x \ll v_{2\omega,g}/\Gamma_{2\omega}$ (the unsaturated limit) and $x \gg {}_{2\omega,g}/\Gamma_{2\omega}$ (the saturated limit). We define a saturation length $L_s = v_{2\omega,g}/\Gamma_{2\omega}$; the amplitude of the second-harmonic mode becomes

$$E_2(x) = -i\frac{\omega E_1^2 D_0}{v_{2\omega,g}}x, \qquad x \ll L_s, \quad (33a)$$

$$E_2(x) = -i\frac{\omega E_1^2 D_0}{\Gamma_{2\omega}}, \qquad x \gg L_s. \quad (33b)$$

In the unsaturated limit we collect light along the x direction. In the saturated limit, however, we let the photons leak through and then collect them along the z direction.

In the second case, the two fundamental frequency modes propagate along the opposite x direction, $K_1(\omega) = -K_2(\omega)$ and $K(2\omega) = 0$, and the second-harmonic photons are collected after leaking out along the z direction. We call this case SHG configuration II. Because of the undepleted-pump approximation and symmetry considerations, we can require $E_2(x)$ to be a constant and obtain

$$E_2 = -i\frac{\omega E_1^2 D_0}{\Gamma_{2\omega}}. \quad (34)$$

Notice that this result is the same as that of saturated SHG configuration I.

To calculate the efficiency of the SHG in a CROW, we still need to relate the power flux to the amplitude of the waveguide mode. Recall that the electromagnetic energy density for a waveguide mode in Eqs. (26) is $|E|^2\epsilon(\mathbf{r})\mathbf{u}_K^*(\mathbf{r})\cdot\mathbf{u}_K(\mathbf{r})/8\pi$. After integration, the energy stored in a unit cell is found to be simply $|E|^2/8\pi$. Consequently, for the waveguide mode propagating along the x direction, the power flux P is given by

$$P = \frac{1}{8\pi}\frac{v_g}{R}|E|^2. \quad (35)$$

For the mode leaking through the z direction, however, the power flux is

$$P = \frac{1}{8\pi}N\Gamma|E|^2, \quad (36)$$

where N is the total number of the resonators in the CROW. Finally, assuming that the total length of the CROW is L and combining Eqs. (35) and (36) with Eqs. (33) and (34), we can obtain the SHG efficiency η_{SHG}. For the unsaturated limit of SHG configuration I, η_{SHG} is

$$\eta_{\mathrm{SHG}} = \frac{P_{2\omega}}{P_\omega} = \frac{1}{v_{2\omega,g}v_{\omega,g}^2}\omega^2|D_0|^2 8\pi R P_\omega L^2. \quad (37)$$

The η_{SHG} for both saturated SHG configuration I and SHG configuration II becomes

$$\eta_{\mathrm{SHG}} = \frac{P_{2\omega}}{P_\omega} = \frac{1}{\Gamma_{2\omega}v_{\omega,g}^2}\omega^2|D_0|^2 8\pi R P_\omega L. \quad (38)$$

The factor $1/v_{\omega,g}^2$ was predicted in Ref. 3 and came directly from the group-velocity argument of the fundamental frequency mode. However, the extra factor $1/v_{2\omega,g}$ or $1/\Gamma_{2\omega}$ cannot be obtained from that simple argument, which suggests that SHG efficiency can be further enhanced if we can slow down the second-harmonic mode or make its effective Q extremely high. Another interesting point is that η_{SHG} is proportional to L^2 in Eq. (37) and is proportional to L only in Eq. (38). The reason for this is that, if we collect second-harmonic photons along the x axis, the phase-matching condition guarantees that the photons generated at different resonators interfere coherently with each other. However, such phase coherence is lost if we collect the photons from the z direction.

5. SUMMARY

We have analyzed two types of CROW, the coupled defect-cavity waveguide and the coupled-microdisk waveguide, using both the tight-binding approximation and the FDTD numerical simulation. In both approaches we found that the dispersion relation of the CROW band can be described by a small coupling coefficient κ. The results for the coupling coefficient κ from the two approaches were compared. The deviation is likely caused by the fact that in the tight-binding approximation we assumed that the single-resonator mode is a real function. We also found that, within each individual resonator of CROW, the waveguide modes are locally essentially the same as the high-Q modes of the single optical resonators. This property enabled us to construct waveguide intersections without cross talk. We also investigated theoretically the SHG process in the CROW under some general approximations. The phase-matching condition in the CROW was derived, and the SHG efficiency η_{SHG} was calculated for two types of SHG configuration. We found that we could further enhance the efficiency of the SHG process by slowing the second-harmonic mode or making its effective Q very high.

APPENDIX A

Assume that we have a Hermitian operator $\mathcal{H}(K)$, which is a function of K. Also, we have the following generalized eigenvalue problem:

$$\mathcal{H}(K)\mathbf{u}_K(\mathbf{r}) = \lambda(K)\epsilon(\mathbf{r})\mathbf{u}_K(\mathbf{r}). \tag{A1}$$

The eigenvalue λ is of course a function of K. We also require that the eigenfunction $\mathbf{u}_K(\mathbf{r})$ be properly normalized as

$$\int_V \mathrm{d}\mathbf{r}\epsilon(\mathbf{r})\mathbf{u}_K^* \cdot \mathbf{u}_K = 1. \tag{A2}$$

The derivative of this normalization relation gives

$$\int_V \mathrm{d}\mathbf{r}\epsilon(\mathbf{r})\left(\frac{\mathrm{d}\mathbf{u}_K^*}{\mathrm{d}K} \cdot \mathbf{u}_K + \mathbf{u}_K^* \cdot \frac{\mathrm{d}\mathbf{u}_K}{\mathrm{d}K}\right) = 0. \tag{A3}$$

The derivative of eigenvalue $\lambda(K)$ can also be found from Eq. (A1) to be

$$\frac{\mathrm{d}\lambda(K)}{\mathrm{d}K} = \int_V \mathrm{d}\mathbf{r}\left[\frac{\mathrm{d}\mathbf{u}_K^*}{\mathrm{d}K} \cdot \mathcal{H}(K)\mathbf{u}_K + \mathbf{u}_K^* \cdot \mathcal{H}(K)\frac{\mathrm{d}\mathbf{u}_K}{\mathrm{d}K} + \mathbf{u}_K^* \cdot \frac{\mathcal{H}(K)}{\mathrm{d}K}\mathbf{u}_K\right]. \tag{A4}$$

Using Eq. (A3) and the fact that $\mathcal{H}(K)$ is a Hermitian operator, we reduce the derivative $\mathrm{d}\lambda/\mathrm{d}K$ to

$$\frac{\mathrm{d}\lambda(K)}{\mathrm{d}K} = \int_V \mathrm{d}\mathbf{r}\mathbf{u}_K^* \cdot \frac{\mathcal{H}(K)}{\mathrm{d}K}\mathbf{u}_K. \tag{A5}$$

This result is a direct generalization of the Hellman–Feynman theorem[33] and can be readily applied to the electromagnetic problem.

As we mentioned in Section 4, by combining Eqs. (22) and (23) and considering the real part, we found an eigenequation for the Bloch wave function $\mathbf{u}_K$:

$$\mathcal{H}_K\mathbf{u}_K(\mathbf{r}) = \frac{\omega^2}{c^2}\epsilon(\mathbf{r})\mathbf{u}_K(\mathbf{r}), \tag{A6a}$$

$$\mathcal{H}_K\mathbf{u}_K = \nabla \times [\nabla \times \mathbf{u}_K] - iK\{\nabla \times [\mathbf{e}_x \times \mathbf{u}_K] + \mathbf{e}_x \times [\nabla \times \mathbf{u}_K]\} - K^2\mathbf{e}_x \times [e_x \times \mathbf{u}_K]. \tag{A6b}$$

It can easily be shown that $\mathcal{H}_K$ is a Hermitian operator. Identifying Eq. (A1) with Eq. (A6a) and $\lambda(K)$ with ω^2/c^2 and using Eq. (A5), we find an expression for the group velocity $\mathrm{d}\omega/\mathrm{d}K$, Eq. (25).

ACKNOWLEDGMENTS

This research was sponsored by the U.S. Army Research Office and the U.S. Office of Naval Research. R. K. Lee acknowledges support from the National Science and Engineering Research Council of Canada.

REFERENCES

1. A. Yariv and P. Yeh, *Optical Waves in Crystals* (Wiley, New York, 1984).
2. P. Yeh and A. Yariv, "Bragg reflection waveguides," Opt. Commun. **19**, 427–430 (1976).
3. A. Yariv, Y. Xu, R. K. Lee, and A. Scherer, "Coupled-resonator optical waveguide: a proposal and analysis," Opt. Lett. **24**, 711–713 (1999).
4. R. D. Meade, A. Devenyi, J. D. Joannopoulos, O. L. Alerhand, D. A. Smith, and K. Kash, "Novel applications of photonic band gap materials: low-loss bends and high Q cavities," J. Appl. Phys. **75**, 4753–4755 (1994).
5. P. R. Villeneuve, S. Fan, and J. D. Joannopoulos, "Microcavities in photonic crystals: mode symmetry, tunability, and coupling efficiency," Phys. Rev. B **54**, 7837–7842 (1996).
6. O. Painter, J. Vuckovic, and A. Scherer, "Defect modes of a two-dimensional photonic crystal in an optically thin dielectric slab," J. Opt. Soc. Am. B **16**, 275–285 (1999).
7. S. John, "Strong localization of photons in certain disordered dielectric superlattices," Phys. Rev. Lett. **58**, 2486–2489 (1987).
8. E. Yablonovitch, "Inhibited spontaneous emission in solid-state physics and electronics," Phys. Rev. Lett. **58**, 2059–2062 (1987).
9. J. D. Joannopoulos, R. D. Meade, and J. N. Winn, *Photonic Crystals* (Princeton University, Princeton, N.J., 1995).
10. S. L. McCall, A. F. Levi, R. E. Slusher, S. J. Pearton, and R. L. Logan, "Whispering-gallery mode microdisk lasers," Appl. Phys. Lett. **60**, 289–291 (1992).
11. N. C. Frateschi and A. F. Levi, "The spectrum of microdisk lasers," J. Appl. Phys. **80**, 644–653 (1996).
12. See, for example, N. W. Ashcroft and N. D. Mermin, *Solid State Physics* (Saunders, Philadelphia, Pa., 1976).
13. K. S. Yee, "Numerical solution of initial boundary value problems involving Maxwell's equations in isotropic media," IEEE Trans. Antennas Propag. **AP-14**, 302–307 (1966).
14. A. Taflove, ed. *Advances in Computational Electromagnetics: the Finite Difference Time Domain Method* (Artech House, Boston, Mass., 1998).
15. K. Sakoda and K. Ohtaka, "Optical response of three-dimensional photonic lattices: solutions of inhomogeneous Maxwell's equations and their applications," Phys. Rev. B **54**, 5732–5741 (1996).
16. K. Sakoda and K. Ohtaka, "Sum-frequency generation in a two-dimensional photonic lattice," Phys. Rev. B **54**, 5742–5749 (1996).
17. M. Scalora, M. J. Bloemer, A. S. Manka, J. P. Dowling, C. M. Bowden, R. Viswanathan, and J. W. Haus, "Pulsed second-harmonic generation in nonlinear, one-dimensional, periodic structures," Phys. Rev. A **56**, 3166–3174 (1997).
18. J. W. Haus, R. Viswanathan, M. Scalora, A. G. Kalocsai, J. D. Cole, and J. Theimer, "Enhanced second-harmonic gen-

eration in media with a weak periodicity," Phys. Rev. A **57**, 2120–2128 (1998).
19. J. N. Winn, S. Fan, J. D. Joannopoulos, and E. P. Ippen, "Interband transitions in photonic crystals," Phys. Rev. B **59**, 1551–1554 (1999).
20. J. Martorell and R. Corbalan, "Enhancement of second harmonic generation in a periodic structure with a defect," Opt. Commun. **108**, 319–323 (1994).
21. J. Trull, R. Vilaseca, J. Martorell, and R. Corbalan, "Second-harmonic generation in local modes of a truncated periodic structure," Opt. Lett. **20**, 1746–1748 (1995).
22. T. Hattori, N. Tsurumachi, and H. Nakatsuka, "Analysis of optical nonlinearity by defect states in one-dimensional photonic crystals," J. Opt. Soc. Am. B **14**, 348–355 (1997).
23. J. P. Dowling, M. Scalora, M. J. Bloemer, and C. M. Bowden, "The photonic band edge laser: a new approach to gain enhancement," J. Appl. Phys. **75**, 1896–1899 (1994).
24. K. Sakoda, "Enhanced light amplification due to group-velocity anomaly peculiar to two- and three-dimensional photonic crystals," Opt. Expr. **4**, 167–176 (1999).
25. M. Scalora, R. J. Flynn, S. B. Reinhardt, R. L. Fork, M. J. Bloemer, M. D. Tocci, C. M. Bowden, H. S. Ledbetter, J. M. Bendickson, J. P. Dowling, and R. P. Leavitt, "Ultrashort pulse propagation at the photonic band edge: large tunable group delay with minimal distortion and loss," Phys. Rev. E **54**, 1078–1081 (1996).
26. X. Feng and Y. Arakawa, "Off-plane angle dependence of photonic band gap in a two-dimensional photonic crystal," IEEE J. Quantum Electron. **32**, 535–542 (1996).
27. G. Mur, "Absorbing boundary conditions for the finite-difference approximation of the time-domain electromagnetic-field equations," IEEE Trans. Electromagn. Compat. **EMC-23**, 377–382 (1981).
28. J. P. Berenger, "A perfectly matched layer for the absorption of electromagnetic waves," J. Comput. Phys. **114**, 185–200 (1994).
29. S. D. Gedney, "An anisotropic perfectly matched layer-absorbing medium for the truncation of FDTD lattices," IEEE Trans. Antennas Propag. **44**, 1630–1639 (1996).
30. See, for example, J. Mathews and R. L. Walker, *Mathematical Methods of Physics* (Wiley, New York, 1970).
31. S. G. Johnson, C. Manolatou, S. Fan, P. Villeneuve, J. D. Joannopoulos, and H. A. Haus, "Elimination of cross talk in waveguide intersections," Opt. Lett. **23**, 1855–1857 (1998).
32. A. Yariv, *Optical Electronics in Modern Communications* (Oxford U. Press, New York, 1997).
33. See, for example, C. Cohen-Tannoudji, B. Piu, and F. Laloe, *Quantum Mechanics* (Wiley, New York, 1977).